The Spine Journal 19 (2019) 1885−1898

Basic Science

Does implantation site influence bone ingrowth into 3D-printed porous implants?

William R. Walsh, BA Biol, BA Chem, PhD[a,b,*], Matthew H. Pelletier, PhD[a,b], Tian Wang, PhD[a,b], Vedran Lovric, PhD[a,b], Per Morberg, MD, PhD[a,c], Ralph J. Mobbs, MBBS, FRACS[a,b,d]

[a] Surgical and Orthopaedic Research Laboratories (SORL), Prince of Wales Clinical School, University of New South Wales, Sydney, Australia
[b] NeuroSpine Surgery Research Group (NSURG), Sydney, Australia
[c] Department of Surgical and Perioperative Sciences, Umea University, Umeå, Sweden
[d] Prince of Wales Private Hospital, Sydney, Australia
Received 6 April 2019; accepted 21 June 2019

Abstract

BACKGROUND CONTEXT: The potential for osseointegration to provide biological fixation for implants may be related to anatomical site and loading conditions.
PURPOSE: To evaluate the influence of anatomical site on osseointegration of 3D-printed implants.
STUDY DESIGN: A comparative preclinical study was performed evaluating bone ingrowth in cortical and cancellous sites in long bones as well as lumbar interbody fusion with posterior pedicle screw stabilization using the same 3D-printed titanium alloy design.
METHODS: 3D-printed dowels were implanted in cortical bone and cancellous bone in adult sheep and evaluated at 4 and 12 weeks for bone ingrowth using radiography, mechanical testing, and histology/histomorphometry. In addition, a single-level lumbar interbody fusion using cages based on the same 3D-printed design was performed. The aperture was filled with autograft or ovine allograft processed with supercritical carbon dioxide. Interbody fusions were assessed at 12 weeks via radiography, mechanical testing, and histology/histomorphometry.
RESULTS: Bone ingrowth in long bone cortical and cancellous sites did not translate directly to interbody fusion cages. While bone ingrowth was robust and improved with time in cortical sites with a line-to-line implantation condition, the same response was not found in cancellous sites even when the implants were placed in a press fit manner. Osseointegration into the porous walls with 3D porous interbody cages was similar to the cancellous implantation sites rather than the cortical sites. The porous domains of the 3D-printed device, in general, were filled with fibrovascular tissue while some bone integration into the porous cages was found at 12 weeks when fusion within the aperture was present.
CONCLUSION: Anatomical site, surgical preparation, biomechanical loading, and graft material play an important role in in vivo response. Bone ingrowth in long bone cortical and cancellous sites does not translate directly to interbody fusions.

Keywords: Additive manufacturing; Animal model; Bone ingrowth; Histology; Interbody fusion; 3D printing

FDA device/drug status: approved (Structural Titanium, Signus, Germany).

Author disclosures: ***WRW***: Grant: Signus, Germany (D). ***MHP***: Nothing to disclose. ***TW***: Nothing to disclose. ***VL***: Nothing to disclose. ***PM***: Nothing to disclose. ***RJM***: Royalties: Stryker (F), A_Spine ASIA (B), Kasios Biomaterials (B); Stock Ownership: Medtronic (B), Johnson&Johnson (B); Consulting: Medacta (B); Grants: NHMRC/Success Trial (I); Fellowship Support: Synthes (C).

* Corresponding author. Surgical and Orthopaedic Research Laboratories (SORL), Prince of Wales Hospital, L1 Clinical Science Bldg, Randwick, NSW 2031, Australia. Tel.: +61 (0)2 9382 2663.

E-mail addresses: W.Walsh@unsw.edu.au, wrwalshau@gmail.com (W.R. Walsh).

https://doi.org/10.1016/j.spinee.2019.06.020
1529-9430/

Introduction

Achieving implant stability through osseointegration or bone formation on or within an implant surface is far from a new or novel concept and been applied in clinical applications in dental [1−7] and orthopedic implants [8−12] for decades. Implant design, material, and surface properties play an important role when choosing a spinal implant [13,14]. Additional variables to be considered include anatomical location, patient-related comorbidities such as diabetes and smoking, surgical site preparation including endplate decortication, implant size, and placement to achieve initial fixation and promote fusion and achieve a clinically acceptable result. Considering the differences between static and dynamic biomechanical loading requirements, in vivo kinematics and surgical and patient-related factors, designing a single geometry to satisfy all applications, remain a challenge.

Historically, osseointegration has been defined as "a direct and functional connection between ordered living bone and the surface of a load-carrying implant" [15] and can be achieved via *ongrowth* or *ingrowth* at the bone-implant interface. Bone ongrowth requires new bone formation directly on the surface of an implant, ideally without an intervening fibrous tissue layer that could influence local mechanical loading or biology and ultimately negatively impact implant longevity and clinical efficacy. Bone ingrowth provides the opportunity of new bone formation on the surface of an implant as well as into the irregular surface or porous domains of an implant [11]. Bone ongrowth and ingrowth have been intensely investigated and have shown to be influenced by factors including material, design, surface parameters, chemistry, coatings, and local biology [8,12,16−26]. From the early days of porous pure titanium meshes [27], ceramic materials including silicon nitride [28,29], sintered beads [12,30,31], porous tantalum devices [9,32,33], or modified PEEK devices [25,34−39] advance to encourage osseointegration continue to develop, often moving forward traditional manufacturing techniques at the same time. Additive manufacturing (3D printing) is one such manufacturing method that can be used to create complex geometries that would be difficult to produce using traditional manufacturing from a cost or complexity perspective [40].

While cell culture experiments can provide valuable information on cellular response, limitations in the complex biological and mechanical environment of an implant in a healing environment cannot be replicated in vitro. Preclinically, large animal models are often used to evaluate the influence of implant surface technologies, coatings, modifications, or materials to assist in guiding the implant design process, regulatory approvals, and clinical applications related to the bone-implant interface and interbody fusion [25,37,38,41−47]. Large animal models allow the use of hardware, graft materials, and surgical procedures which in certain aspects can translate well to the human clinical scenario, or not, depending how the study is performed. Large animal models are not without shortcomings and can be limiting or over-interpreted when factors such as animal age, implantation site, surgical preparation, implant size, as well as biomechanical factors related to load bearing of the site and stability are not considered.

The current study examined the in vivo results of a porous titanium implant manufactured using Selective Laser Melting to produce cylindrical dowels in cancellous and cortical sites and as a porous interbody lumbar spinal fusion cage. We sought to determine if osseointegration in porous implants in long bone defects in cortical or cancellous bone can be applied to interbody fusion. The null hypothesis of the current study was that the implant location would not influence osseointegration of the 3D-printed titanium implant design.

Methods

This study utilized two large animal models in sheep. A well-reported bone ingrowth model used to evaluate different implant materials, coatings, and technology for osseointegration in cortical and cancellous sites [12,16−19,22,24,48] and an endplate-sparing interbody fusion model [43] with posterior pedicle screw fixation [49−51] to assess a more clinically relevant functional model. The interbody cages were filled with autograft or allograft as detailed below.

Implants

Titanium alloy (Ti6AL4V) implants were prepared using Selective Laser Melting and the 3D implant architecture of the ST interbody cage ("Structural Titanium," Signus, Germany). The ST cage is an open-pore diamond grid structure. Cylindrical dowels of the same design (6.0 mm diameter × 25 mm long) were prepared for implantation in the cancellous bone and cortical bone. Interbody cages (4.5 mm high, 10 mm wide, and 20 mm long) with a central aperture used to fill with graft material were printed to fit the sheep L4−L5 interbody space to allow for a clinically realistic implantation rather than violating the endplate at the time of surgery to accommodate an oversized cage [43]. A cylindrical dowel and interbody fusion implant were examined using stereo-zoom microscopy using a Leica M125C Stereo Microscope (Leica, Germany) and environmental electron microscopy (Hitachi TM1000, Japan) to assess implant architecture and surface characteristics of the implants (Fig. 1).

Supercritical fluid-treated ovine allograft

Ovine allograft was prepared using the same process used for human corticocancellous bone with supercritical fluid (Australian Biotechnologies, Frenchs Forest, Australia) (Fig. 2). Fresh cadaveric ovine humeral heads from 2-year-old wethers were harvested and morselized to

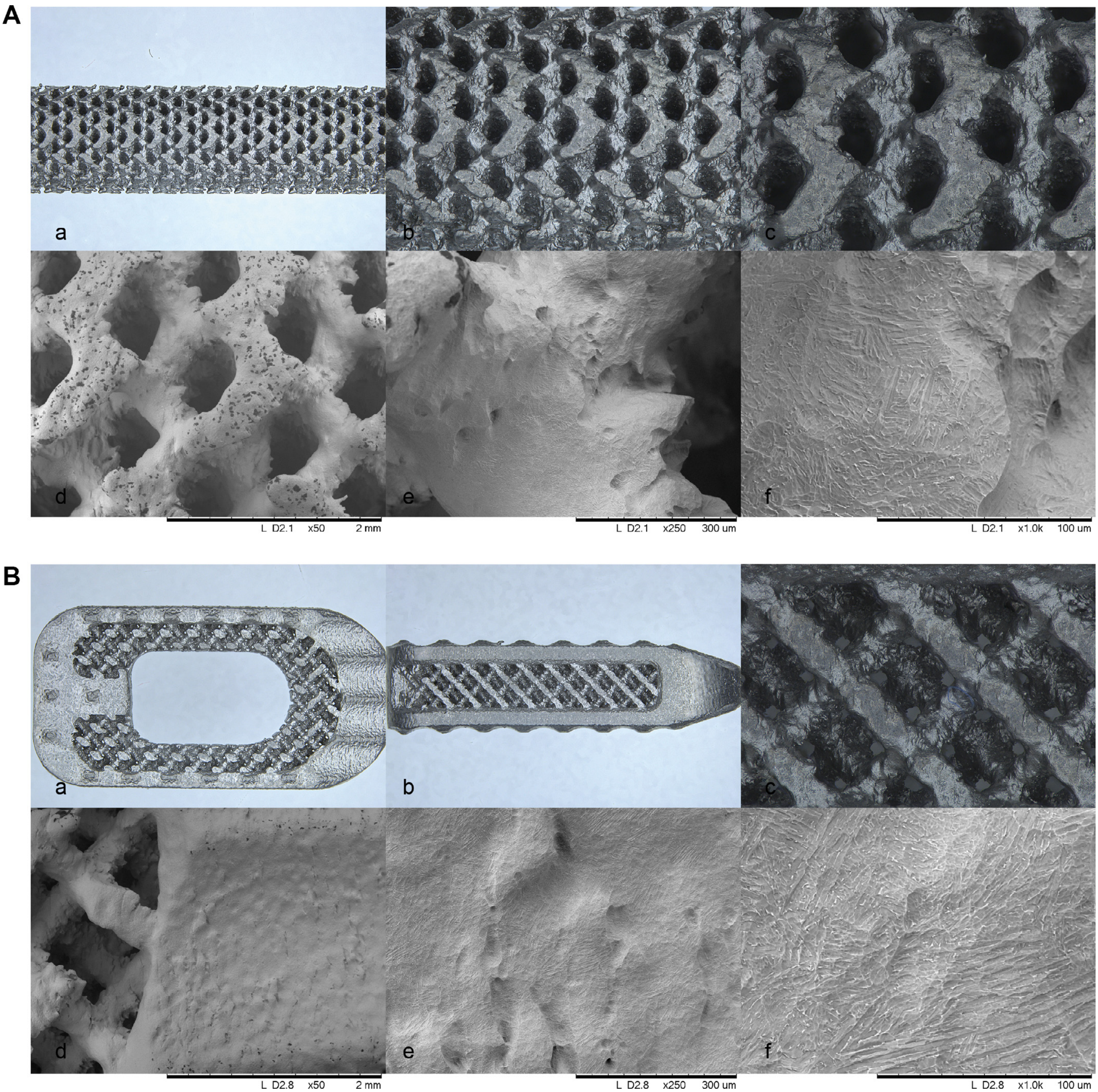

Fig. 1. (A) Titanium alloy (Ti6AL4V) dowels (6.0 mm diameter × 25 mm long) were prepared using Selective Laser Melting using an open-pore diamond grid structure of the ST interbody cage ("Structural Titanium," Signus, Germany). Light microscopy (a−c) and environmental SEM (d−f) revealed the 3D structure as well as the surface topography which was also found in the interbody cages (B). (B) Titanium alloy (Ti6AL4V) ST interbody cage ("Structural Titanium," Signus, Germany) (4.5 mm high, 10 mm wide, and 20 mm long) were prepared using Selective Laser Melting using an open-pore diamond grid structure. Light microscopy (a−c) and environmental SEM (d−f) revealed the 3D structure as well as the surface topography which was also found in the bone dowels (A).

produce corticocancellous graft using a hand-operated bone mill (Noviomagus, Spierings Orthopaedics BV, Nijmegen, the Netherlands) and sieved to collect particles 1 to 2 mm. Corticocancellous bone particles were packaged into high-density polyethylene pouches and placed into a high-pressure chamber. The bone particles were treated using supercritical carbon dioxide ($SCCO_2$) at 37° and 100 bar for 1 hour to remove excess lipids. Following $SCCO_2$ treatment, the bone was lavaged with warm (37°C) saline, placed in an ultrasonic cleaner for 30 minutes, and subjected to soaks in detergent (Triton X-100), hydrogen peroxide, and isopropyl alcohol under aseptic conditions.

Fig. 2. Fresh ovine humeral heads from skeletally mature cross-bred wethers (A) were harvested and morselized (B,C) into particle form (0.5−1 mm) using a Noviomagus Bone Mill. Bone particles were defatted and cleaned using supercritical fluid technology and a series of washes to remove blood, lipids, and cellular debris. Following packaging (D), bone allograft was terminally sterilized using supercritical fluid technology and a peracetic acid additive.

Corticocancellous bone particles were air dried for 1 hour and packaged before terminal sterilization step using supercritical carbon dioxide ($SCCO_2$) at 37° and 100 bar for 2 hours with peracetic acid additive.

Animal surgical preparation

All surgical procedures were performed following institutional ethical clearance. Pre-emptive analgesic was provided using transdermal fentanyl patches 24 hours before surgery (Christou, et al. 2015) [52] and to provide smoother sedation and anesthetic induction. Animals were sedated with an intramuscular (IM) injection of Xylazine (0.2 mg/kg) followed by Ketamine IM (6 mg/kg) 15 minutes later. All animals received 1 g of Cephalothin (18−22 mg/kg) intravenously and 5 mL oxytetracycline (200 mg/mL) at 18 to 22 mg/kg intramuscularly. Benacillin (Procaine penicillin 150 mg/mL) 1 mL/10 kg was given IM. The transdermal fentanyl patches were replaced with new ones (to provide a minimum of 72 hours of postoperative analgesia) and Carprofen (Rimadyl 50 mg/mL) at 3 to 4 mg/kg IM given before surgery. Animals were transferred to the operating room table and anesthesia maintained using on isoflurane (1.5%−3%) and oxygen (2 L/min) throughout the procedures.

Bone ingrowth model

Ten dowels (two cancellous and three bicortical implants per side) were implanted using an established osseointegration model in two adult cross bred wethers [12,16−19,22,24,48]. Dowels were placed in a press fit manner (6.0 mm implants in a 5.5 mm drill hole) in the cancellous bone of medial distal femoral condyles and proximal tibias (Fig. 3). A 4.5 mm three-fluted drill (Surgibit, Orthopedic Innovations, Sydney) was used created a pilot hole followed by a 5.5 mm diameter drill-bit. Dowels in the cortical bone were placed in the diaphysis of the tibia in a line to line manner (6 mm implant in a 6 mm hole) using the 4.5 mm followed by a 6 mm diameter drill-bit to create three bicortical defects in the tibial diaphysis. The periosteum, soft tissues, and dermis were closed in layers using 3-0 and 2-0 resorbable suture, respectively. One animal was euthanized via lethal intravenous overdose of sodium pentobarbitone (Lethabarb, Virbac; 1 mL/2 kg) following sedation at 4 weeks and one at 12 weeks. The right and left tibias and femurs were harvested for endpoints.

Single-level interbody fusion with bilateral posterior pedicle screws

A single-level (L4−L5) interbody fusion as reported by Bae et al. [43] was performed in eight 4- to 5-year-old ewes with the addition posterior pedicle screw fixation. Four animals received iliac crest corticocancellous autograft harvested from the right ilium using a rongeur. The autograft was placed in a sterile bowl and morselized into 1 to 2 mm pieces for implantation into the aperture of the interbody cage. Ovine allograft (1−2 mm pieces) manufactured as described was used in four animals.

The L4−L5 interbody fusion level was approached laterally using blunt dissection to palpate the disc. Gelpi

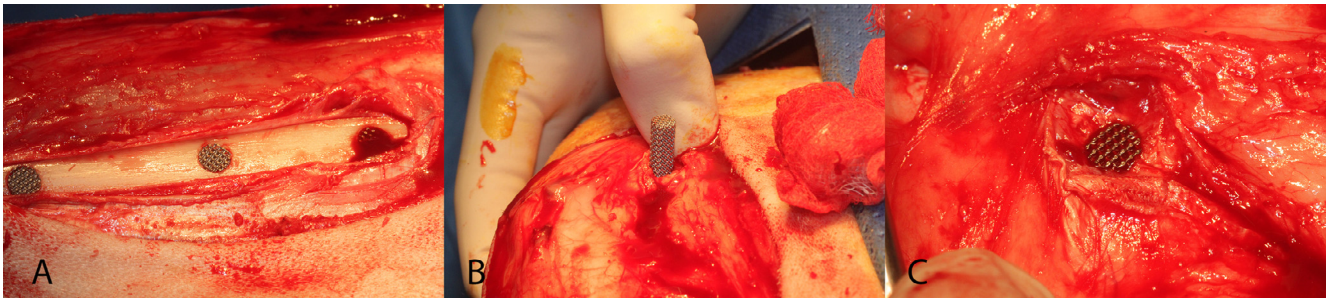

Fig. 3. Dowels in the cortical bone (A) were placed in the diaphysis of the tibia in a line to line manner (6 mm implant in a 6 mm hole) using the 4.5 mm followed by a 6 mm diameter drill-bit to create three bicortical defects in the tibial diaphysis. Dowels were placed in a press fit manner (6.0 mm implants in a 5.5 mm drill hole) in the cancellous bone of medial distal femoral condyles (B,C) and proximal tibias.

retractors were used to visualize the lateral annulus which was removed with sharp dissection. A tear drop curette was used to mobilize and remove the nucleus pulposus. A rasp prepared the endplates and removes remaining nucleus pulposus and avoided endplate damage [43]. The interbody devices were filled with the graft materials (Fig. 4) and inserted into the disc space using an impactor. The soft tissues were reapposed, and the skin closed in layers. Following the completion of the interbody fusion surgery, the animals were repositioned in the prone position and titanium pedicle screws (5.0 mm × 35 mm) with a 5.5 mm titanium rods (Wiltrom, Taiwan) placed bilaterally at the L4−L5 levels for posterior fixation [49−51] (Fig. 4). Interbody fusion animals were euthanized at 12 weeks and the lumbar spine harvested for radiographs, microcomputed tomography, robotic range of motion (ROM), and polymethylmethacrylate (PMMA) histology.

Harvest

Dowels implanted in cancellous bone of the distal femur and proximal tibia were isolated using a saw and fixed in cold phosphate-buffered formalin, dehydrated in ethanol and embedded in PMMA for histologic sectioning. Cortical samples were processed for push-out mechanical testing to determine shear strength and PMMA histology to evaluate bone ingrowth. The interbody fusions were harvested at the L4−L5 levels and processed fresh for radiography (Faxitron radiographs and microcomputed tomography), manual palpation and ROM testing.

Radiography

The femur and tibia from the bone ingrowth animals were radiographed in the anteroposterior and lateral views using a Faxitron (Faxitron, Wheeling, IL) and

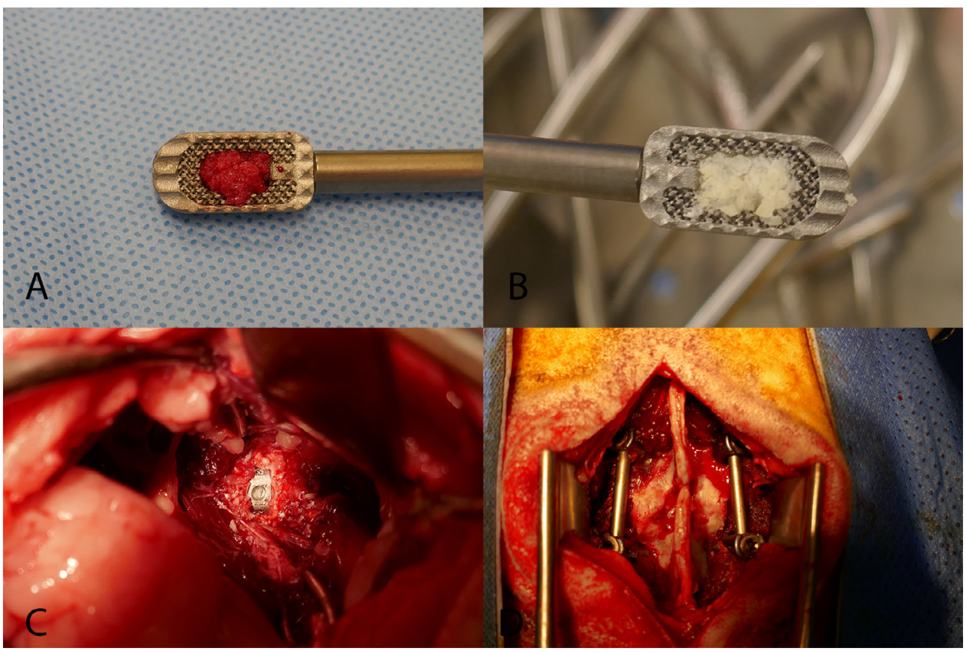

Fig. 4. The aperture of interbody cages was filled with the autograft (A) harvested from the iliac crest or allograft (B) processed using supercritical technology process outlined in Fig. 2. The cages were implanted at the L4−L5 levels using a lateral approach (C) and the animal repositioned in the prone position and titanium pedicle screws placed bilaterally at the L4−L5 levels for posterior fixation (D).

digital plates (AGFA CR MD4.0 Cassette). The Faxitron radiographs were used to examine the status of the 3D dowel-bone interface for any Faxitron radiographic evidence of new bone ingrowth or adverse events. Posteroanterior Faxitron radiographs of the L4−L5 fusions were taken with the rods and pedicle screws as well as following removal of the rods were taken. Microcomputed tomography (μCT) was performed on the spines using an Inveon Scanner (Siemens, USA) with 44 μm resolution. The Faxitron radiographs and micro-CT scans from the interbody fusions were evaluated blinded to graft type (autograft vs allograft) for signs of bony integration with the host endplate, new bone formation in the cage aperture, new bone integration into the porous titanium regions of the cage, evidence of cage subsidence, pedicle screw loosening or adverse bony reactions. Micro-CTs were graded in a blinded manner as outlined in Table 1 and analyzed using a Mann-Whitney *U* test using SPSS for Windows.

Mechanical testing: bone ingrowth push-out testing

Dowels implanted in cortical sites were isolated using a bandsaw in the axial plane. These were sectioned in the sagittal plane to isolate a medial site for push-out testing and lateral for histology alone using a Buehler low speed saw and a diamond-coated wafering blade [12,16−19,22,24,48]. Before testing, specimens were polished perpendicular to the implant to remove periosteal bone growth. Implants were tested for implant-bone interface shear strength using a standard push-out test. Specimens were tested at 0.5 mm/min on MTS, a calibrated servo-hydraulic testing machine (MTS Mini Bionix, MTS System Corporation, Eden Prairie, MN). Peak Load (N), energy to peak load (Nmm), and stiffness (N/mm) were obtained from the load versus displacement graphs using a MatLab custom script (MatLab Natick, MA). Shear stress was calculated (eq 1) using cortical thickness measurements obtained from PMMA histology [12,16−19,22,24,48]. The mechanical data between 4 and 12 weeks from the bone dowel testing were analyzed via an unpaired *t* test using SPSS.

$$\sigma = \frac{Load}{\left(\frac{c_1 + c_2}{2}\right).\pi.d_i}$$

Table 1
Radiographic grading scale

Number	Grade	Description
0	No new bone	No new bone formation visible
1	Visible new bone	New bone formation visible but no continuous bone
2	Possible fusion	Continuous bridging new bone formation with visible lucency
3	Probable fusion	Continuous bridging new bone formation

Equation 1: Shear stress calculation where c = cortical thickness measurement from each side of the implant based on the histological slides, d_i = diameter of the implant.

Mechanical testing: interbody fusion

The stability of the L4−L5 fusions was assessed by manual palpation at 12 weeks after removal of the rods. Two trained and experienced blinded observers assessed the fusions in lateral bending and flexion-extension. The fusions were graded as either fused (rigid, no movement) or not fused (not rigid, movement detected) compared to the untreated level above was as a relative comparison. Manual palpation data were analyzed using a Mann-Whitney *U* test using SPSS for Windows.

The L4−L5 segments were potted following manual palpation with a smooth cast 300 resin (Smooth-On, Macungie, PA) in an aluminum potting cylinder. ROM in flexion-extension, lateral bending, and axial rotation was measured using a robotic 6° of freedom musculoskeletal simulator, simVITRO (Simulation Solutions and Cleveland Clinic, Ohio) nondestructively to ±7.5 Nm. Each loading profile was repeated 4.5 times and the mean value for ROM of the last three cycles was used for statistical comparison. ROM data were analyzed using an in-house custom MatLab script and statistically using an unpaired *t* test using SPSS. Fusions were then fixed in phosphate-buffered formalin for PMMA histology.

PMMA histology and histomorphometry

All samples (dowels and interbody fusions) were processed using established hard tissue histology techniques using PMMA [12,16−19,22,24,37,48]. Formalin-fixed samples were sequentially dehydrated in increasing concentrations of ethanol before infiltration in methylmethacrylate and polymerization.

Embedded cortical and cancellous dowels were sectioned along the long axis of the implants using a Leica SP 1600 Microtome. A minimum of two thin (~15−20 micron) sections were cut from each dowel. The interbody fusions were sectioned in the sagittal plane in three sites (sections ~15 micron thick). The sections were briefly etched in acidic ethanol (98 mL ethanol 96% and 2 mL HCl 37%) and stained with methylene blue followed by basic fuchsin [53]. The staining results in bone staining pink, fibrous tissue blue/purple.

The stained slides were reviewed under low magnification to provide an overview of the section and histomorphometry. The implant-bone interface and local reactions were carefully examined at higher magnification for the presence of inflammatory cells or local particulate in the cancellous, cortical, or interbody sites. The interbody fusion slides were evaluated in a blinded manner to examine the status of the endplates to the interbody cage, tissue integration into the porous domains of the interbody cage as well as fusion response to the graft material (autograft of allograft) used inside the aperture.

Histomorphometry

The low-magnification PMMA histology was used for the determination of bone ingrowth into the dowels implanted in cancellous and cortical sites at 4 and 12 weeks and the interbody fusion at 12 weeks using MatLab to determine the amount of substrate, new bone, and bone in the available void based on established methods [16−18]. A region of interest for each image using a polygon technique to specifically examine the implant-bone interface was employed. The 3D-printed metal, mineralized bone, bone marrow, or fibrous tissue was identified by pixel color and morphology and the area determined as a percentage of the region of interest in the sites. The same procedure was performed for the porous walls of the interbody cage to determine the amount of bone ingrowth into the cage. Bone in the available void in the porous 3D-printed implants was determined by the new bone within the porous implants divided by the available void which was calculated by the total area minus the amount of metal in the section. Histomorphometric data were analyzed using an unpaired *t* test using SPSS.

Results

Implants

Macroscopic light microscopy and environmental scanning electron microscopy revealed the similar porous domains and surface topography of the dowels and interbody fusion cages (Fig. 1) both produced the same Selective Laser Melting process.

Surgery and in-life

Surgery was successfully completed on all animals in the bone ingrowth dowel model (Fig. 2) as well as the interbody fusion (Fig. 4). The interbody cages retained the autograft and supercritical fluid-treated allograft well and were easily implanted. The allograft appeared white, consistent with processing with supercritical carbon dioxide and removal of lipids and organic debris in the allograft (Figs. 2D and 4B).

No adverse events were noted in the in-life phase of the study. No evidence of infection or adverse reactions were observed at the time of harvest of the dowels from the tibias and femurs at the cancellous or cortical implantation sites at 4 and 12 weeks or the interbody fusions at 12 weeks.

Radiography

Anteroposterior Faxitron radiographs in the tibia cortical sites revealed an increase in signal intensity between 4 and 12 weeks suggesting a progression of bone ingrowth in the cortical sites. Faxitron radiographs at the cancellous sites were difficult to assess due to the presence of normal bone anterior and posterior to the implant (Fig. 5a).

Faxitron posteroanterior radiographs of the interbody fusions at 12 weeks revealed the interbody cages on the host endplates while any new bone ingrowth into the porous implants as well as the presence of a bony fusion from L4 to L5 was difficult to assess (Fig. 5b). Subsidence based on the Faxitron radiographs was not apparent at 12 weeks.

Micro-computed tomography of the interbody fusions revealed the presence of an artefact due to the titanium alloy implants which made the assessment of any bone within the porous domains of the interbody cage uncertain (Fig. 6). Evidence of some bony resorption above the wall of the interbody cage was found in 50% of the cases with both graft materials (Fig. 6).

Micro-computed tomography was used to evaluate the status of the fusion between the levels within the apertures using autograft as well as supercritical fluid-treated allograft with both graft materials demonstrating evidence of a change in signal intensity and some integration with the host endplates supporting a continuous bone bridge between the treated levels. Micro-computed tomography grading at 12 weeks of possible fusion (grade 2) and probable fusion (grade 3) for cages filled with autograft were 1 out 4 and 3 out of 4, respectively, while supercritical fluid-treated allograft-filled cages presented 2 of 4 possible fusions and 2 out of 4 probable fusions. The distribution of these grades did not differ based on the Mann-Whitney *U*test (p=.686). Subsidence based on the micro-computed tomography review was not apparent at 12 weeks.

Mechanical testing

Push-out testing of the tibial cortical dowels at 4 and 12 weeks revealed a significant increase in properties (Table 2). Peak load, energy, stiffness, and shear stress were statistically superior at 12 weeks compared to 4 weeks ($p<.05$).

Manual palpation and ROM

Manual palpation of the spinal fusions revealed a rigid fusion (no movement) in 75% of the cages filled with autograft and 100% of the cages filled with supercritical fluid-treated allograft. The distribution of these grades did not differ based on the Mann-Whitney *U*test (p=.686).

An example of ROM testing in lateral bending, axial rotation, and flexion-extension data output using simVITRO is presented in Fig. 7. Pure bending moments were applied and the resulting angular deformation in all planes was monitored revealing minimal off axis moments. ROM results did not reveal any differences between cages filled with autograft or supercritical fluid-treated allograft (Table 3).

Histology and histomorphometry

Histology in the tibial cortical sites (Fig. 8) demonstrated a progression of normal new bone formation between 4 and

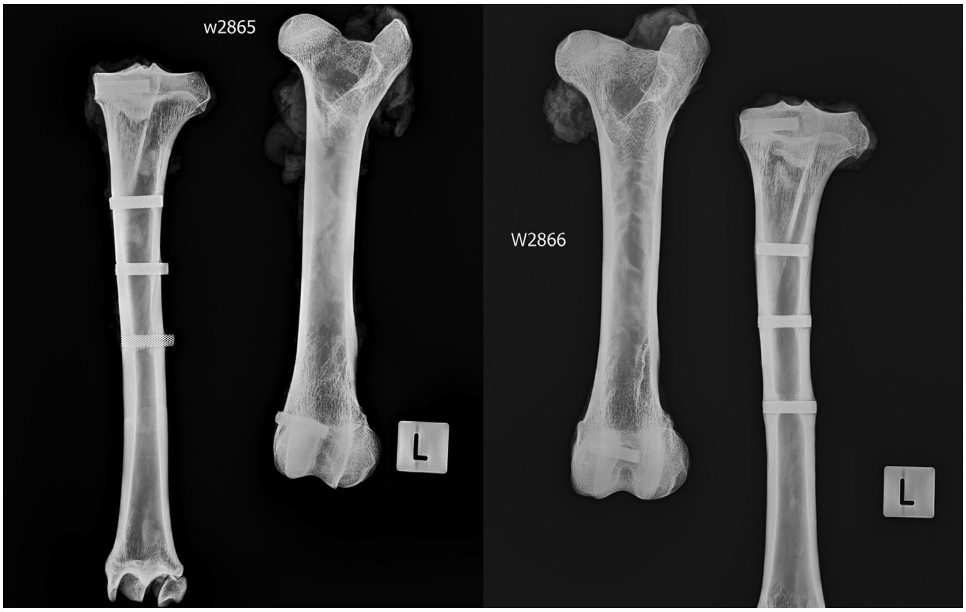

Fig. 5a. Anteroposterior Faxitron radiographs at 4 weeks (W2865) and 12 weeks (W2866) did not reveal any adverse events. Evaluation of new bone within the porous devices was difficult even with high-resolution Faxitron radiographs.

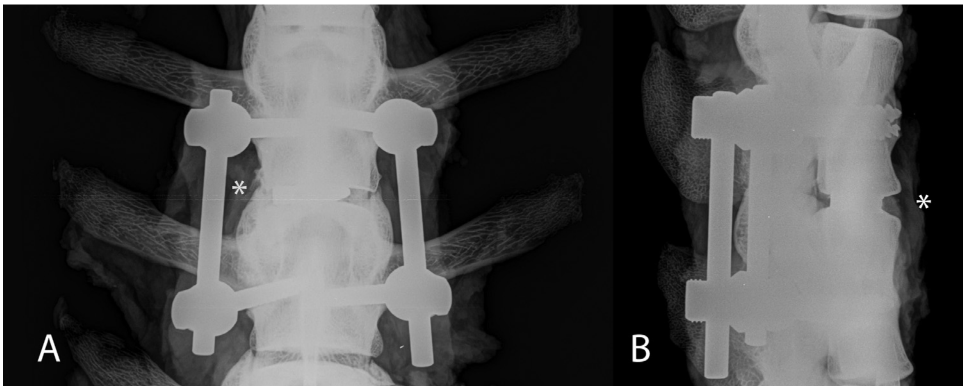

Fig. 5b. Posteroanterior (A) and lateral (B) Faxitron radiographs at 12 weeks of the interbody fusions revealed the presence of the implant (*) and the pedicle screws while detection of bone at the endplate interface or inside the cage itself was not possible.

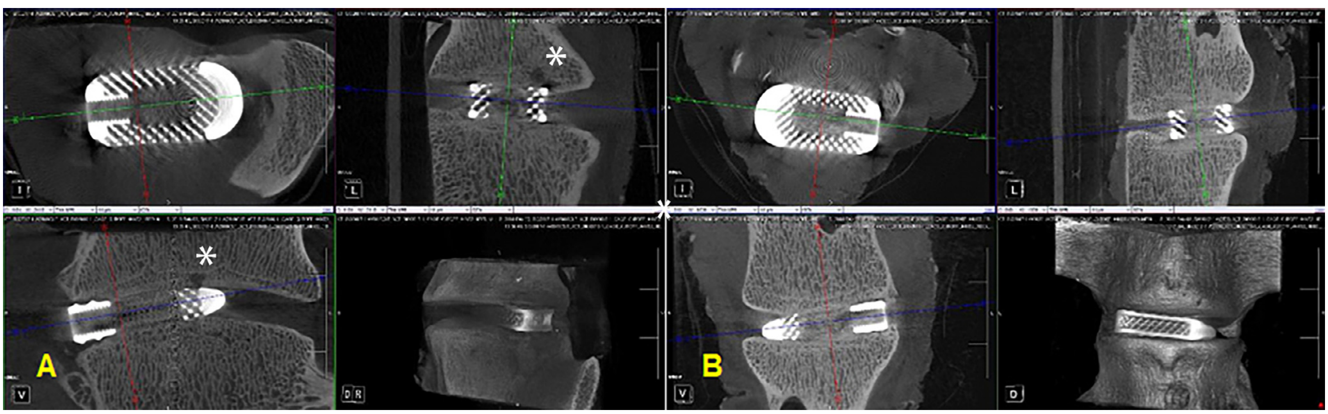

Fig. 6. Micro-computed tomography of the interbody fusions revealed the presence of artefact due to the titanium alloy implants which made assessment of any bone within the porous domains of the interbody cage uncertain. Evidence of some bony resorption (*) above the wall of the interbody cage was found in 50% of the cases with both graft materials.

Table 2
Radiographic grading scale

	Peak force (N)		Energy to failure (Nmm)		Stiffness (N/mm)		Shear stress (N/mm^2)	
Weeks	Mean	Standard deviation	Mean	Standard deviation	Mean	Standard deviation	Mean	Standard deviation
4	752.4	237.17	177.34	72.57	3,032.94	1,302.64	8.91	1.9
12	2,621.59	1,029.86	1,347.83	519.36	4,831.71	2,199.36	31.25	6.84

Table 3
Radiographic grading scale

		Lateral bending (degrees)		Axial rotation (degrees)		Flexion-extension (degrees)	
ROM at 7.5 Nm		Mean	Standard deviation	Mean	Standard deviation	Mean	Standard deviation
Group	Autograft	6.44	1.33	3.69	0.41	6.73	1.16
	SCF allograft	6.59	2.42	3.76	0.91	6.53	2.20

12 weeks with direct bone formation and the lack of any fibrous tissue into the porous domains of the cortical samples. Histology in the cancellous sites (Fig. 8) presented a different temporal finding with some new bone integration at the host margins with the 3D-printed dowels at 4 weeks which did not progress deeper into the porous implants at 12 weeks. Some new bone marrow formed at the bone-implant margins in cancellous sites while the majority of the porous domains were filled with loose connective tissue.

Interbody cage histology (Fig. 9) allowed the examination of the interface between the vertebral endplate and the 3D porous interbody cage, new bone integration into the porous walls of the cage and inside the aperture at 12 weeks. Overall, there was the lack of any inflammatory cells or

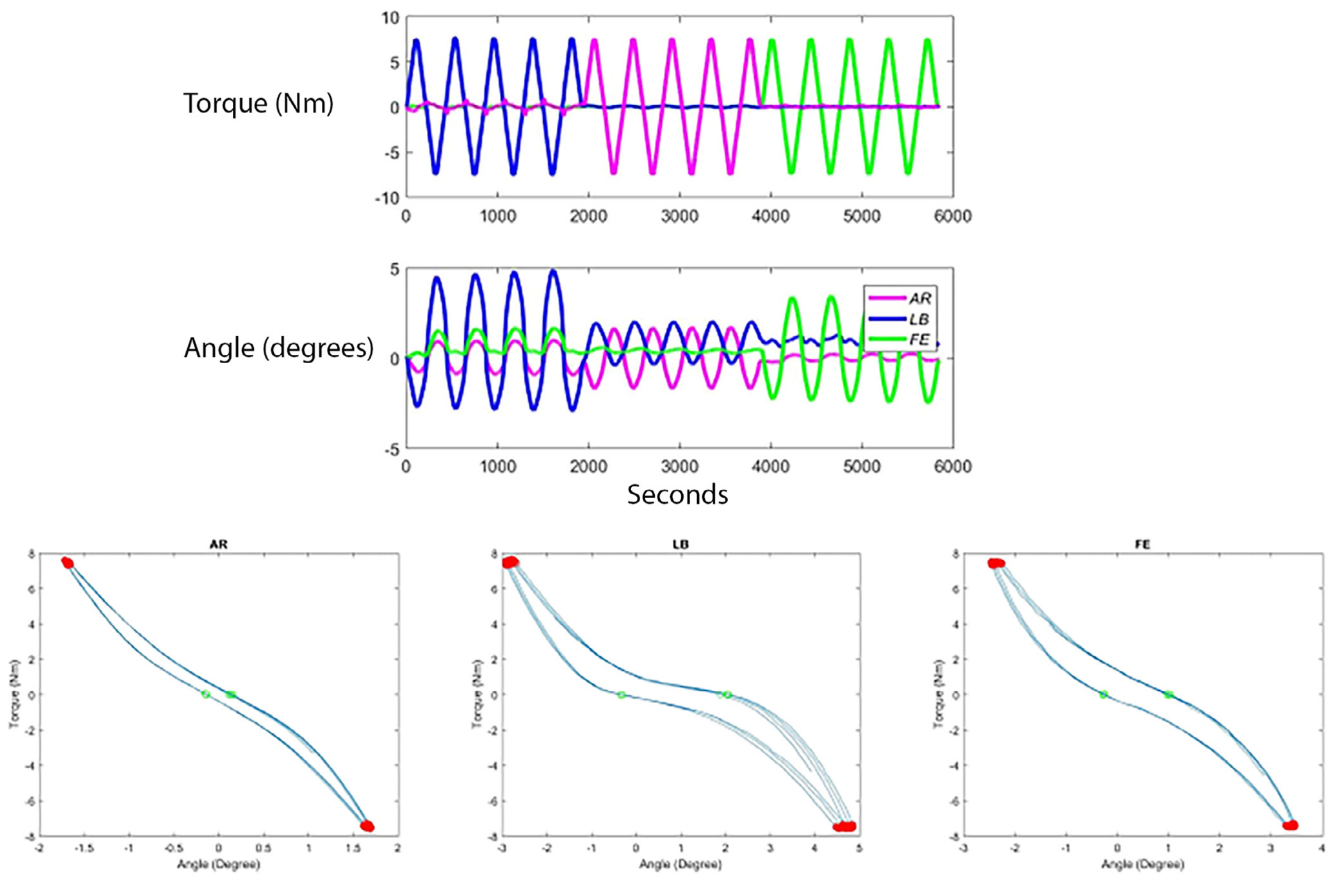

Fig. 7. Range of motion testing using SimVitro applied ±7.5 Nm while monitoring angular deformation in axial rotation, lateral bending, and flexion-extension.

Fig. 8. PMMA histology in the cortical sites at 4 weeks and 12 weeks (A,B) demonstrated a progression in new bone ingrowth into the porous morphology of the 3D-printed bone dowels. Cancellous bone ingrowth at 4 and 12 weeks (C,D) did not progress with time deeper into the porous structure. Some new bone marrow formed at the bone-implant margins in cancellous sites while the majority of the porous domains were filled with loose connective tissue in cancellous sites.

evidence of adverse reaction to the 3D-printed interbody cage or the autograft or supercritical fluid-treated allograft.

The endplates were generally intact with cages placed directly on the host bone. The areas where microcomputed tomography revealed bone resorption were found to have fibrovascular tissue when examined with histology (Fig. 9). Some new bone formation within the 3D porous walls of the interbody cages at the interface of the endplates was found when a continuous fusion within the aperture was present (Fig. 9). Fibrovascular tissue was found in the porous walls of the interbody cages (Figs. 9 and 10) in the absence of a bony fusion within the aperture. Both graft materials demonstrated new bone formation and remodeling in the aperture at 12 weeks (Fig. 9). The osteoconductive nature of autograft and the allograft was apparent with new bone ongrowth and remodeling to the graft materials at 12 weeks combined with fibrovascular tissue. Histologically, a continuous bony bridge within the aperture at 12 weeks was not found with autograft and in only one cage filled with allograft.

Histomorphometry quantification of new bone ingrowth into porous implants in cortical and cancell‘ous sites as well as the porous walls of the interbody cages is presented in Fig. 10. A statistically significant increase was found for new bone formation in cortical sites between 4 and 12 weeks, while an increase in cancellous sites as well as the walls of the interbody cages was not found (Fig. 10). Bone in the available void in dowels implanted in the cortical sites increased from 26% (±11%) at 4 weeks to 74% (±14%) at 12 weeks. Bone in the available void in dowels implanted in cancellous sites at 4 weeks was 14% (±3%) and 15% (±17%) at 12 weeks. Bone in the available void of the walls in the porous interbody cages at 12 weeks was not influenced by the graft material and was 21% (±16%) when the aperture was filled with autograft and 20% (±22%) when the aperture was filled with supercritical fluid-treated allograft (Fig. 11).

Discussion

Osseointegration offers a biological means of implant fixation that can be achieved through a variety of mechanisms including bone ongrowth to a material surface, ingrowth into the porous domains of a material, as well as growth through geometric ultrastructure of a material. Implant fixation or stabilization clearly needs to consider the anatomical site and type of implant and clinical condition being treated. Differences in the surgical approach, soft tissue considerations, bone health and density, kinematics, and mechanical loading are all factors to consider not only for surgeons but for implant designers and manufactures. Considering this complexity, a single material or optimized design to satisfy all clinical and design applications for fixation seems improbable and reflects the wide range of

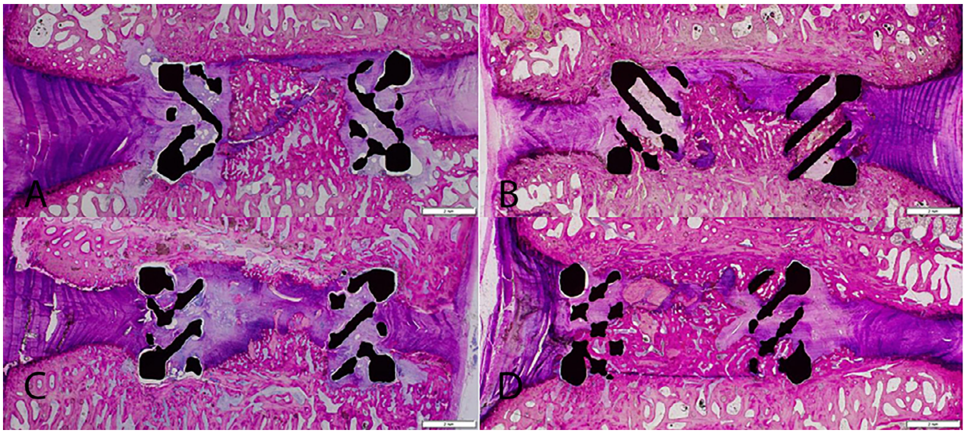

Fig. 9. Interbody cage histology allowed examination of the interface between the vertebral endplate and the 3D porous interbody cage, new bone integration into the porous walls of the cage and inside the aperture at 12 weeks. There was the lack of any inflammatory cells or evidence of adverse reaction to the 3D-printed interbody cage or the autograft (A,C) or supercritical fluid-treated allograft (B,D). The porous walls of the device were primarily filled with fibrous tissue. Some new bone within the porous walls was found at 12 weeks (B,D).

implant technologies available at the bone-implant interface for spinal fusion applications as well as arthroplasty across all joints (hips, knees, shoulders, ankles, and spine). Initial stability in hip and knee arthroplasty can be achieved through a combination of surgical preparation, cement fixation, and implant geometry to aid osseointegration, through bone ongrowth to textured surfaces or coatings or ingrowth into porous domains at the implant-bone interface providing biological fixation. Interbody spinal fusion adds the additional complexity of anatomy, removal of the disc material, avoiding damage to the endplates, mechanical stability, as well as the type, quality, and quantity of graft material used in or around interbody fusion devices.

Modern manufacturing methods continue to evolve in implant design with an aim toward controlling what happens at the bone-implant interface. Altering surface topography and features, coatings as well as porous interfaces through a variety of manufacturing process have shown to

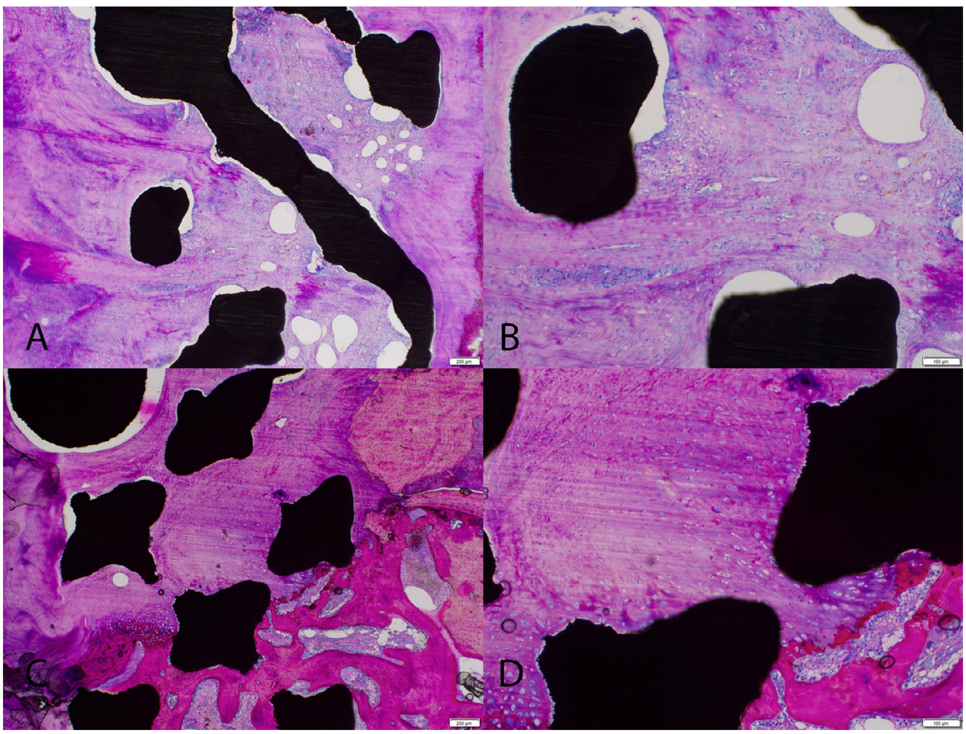

Fig. 10. Higher magnification within the porous walls of the cages at 12 weeks revealed fibrous tissue with autograft in the aperture (A,B) and some new bone at the interface with wall of the cage with supercritical fluid-processed allograft (C,D).

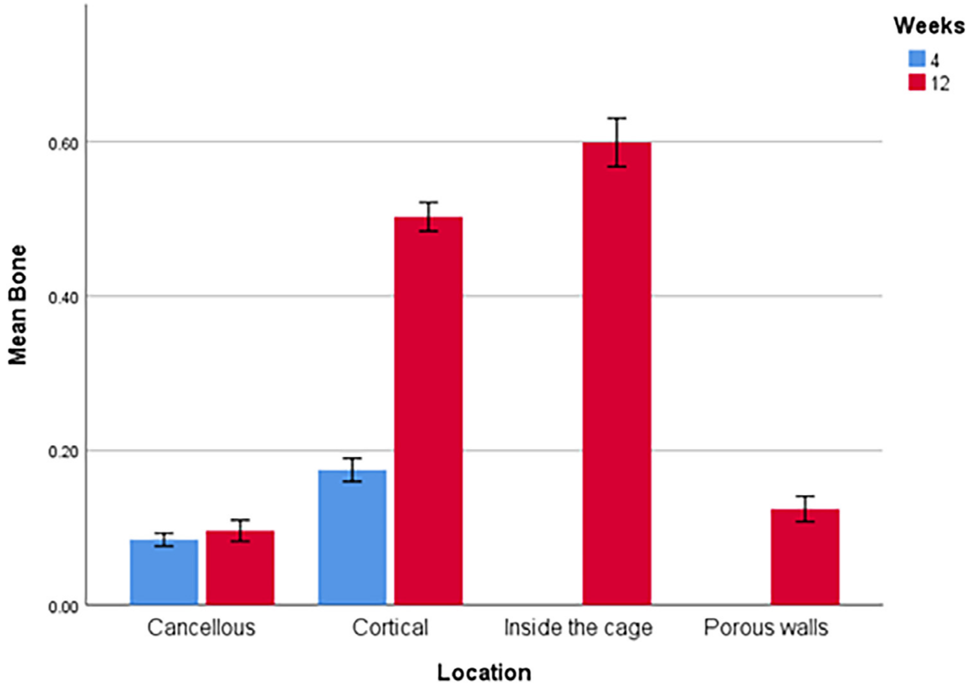

Fig. 11. New bone formation based on histomorphometry within the porous domains of the cancellous implants did not improve with time between 4 and 12 weeks. New bone formation within the porous domains of the cortical implants revealed the statistical increase in bone formation between 4 and 12 weeks. No differences were detected between the amount of bone formation in the cancellous sites compared to the bone ingrowth into the porous domains of the interbody cage at 12 weeks.

influence the bone-implant interface in preclinical and clinical studies [35,54]. Additive manufacturing represents an alternative means of implant production where complex shapes can be produced that would be considered difficult [55] or too expensive to achieve through traditional means. Like all technology, 3D printing continues to advance with improvements in resolution as well as new offerings of materials but can be constrained due commercial and economic pressures. Whether the use of “3D” implants improves clinical outcomes in medicine or influences the socioeconomic aspects of the medical devices industry remains to be proven [56]. The ability to have custom designs which additive manufacturing can facilitate remains an exciting option [55].

The current study explored the in vivo response at the bone-implant interface of the same complex geometry of a porous titanium alloy device manufactured using the Selective Laser Melting implanted in the cortical and cancellous bone as well as in an interbody fusion. The cortical and cancellous implantation model has been reported for more than two decades [12,16−19,22,24,48] in the development of uncemented fixation in hip and knee arthroplasty devices. Autograft and sheep supercritical fluid cancellous allograft was used to fill the aperture of the 3D-printed interbody cages. Human allograft manufactured using the same supercritical fluid carbon dioxide procedure has been shown to facilitate interbody fusions in humans [57,58]. Evaluating the same 3D porous devices in an interbody fusion model allowed us to compare the performance of porous devices with respect to implantation site. We sought to determine if osseointegration in porous implants in long bone defects in cortical or cancellous bone can be applied to interbody fusion. The null hypothesis of the current study was that the implant location would not influence the osseointegration of the 3D-printed porous titanium implant design.

The results of the current study revealed bone ingrowth in long bone cortical and cancellous sites does not translate directly to interbody fusions. While bone ingrowth was robust and improved with time in cortical sites with a line-to-line condition, the same response was not found in cancellous sites where the implants were placed in a press fit manner. We reported similar results in the same bone ingrowth model for a porous scaffold of Ti6Al4V (Regenerex; Biomet) manufactured using electrodischarged machining [17] in cortical sites with extensive osseointegration between 4 and 12 weeks and limited osseointegration in cancellous sites at 4 weeks which did not progress at 12 weeks. Osseointegration in the current study with 3D porous interbody cages was like the cancellous implantation sites rather than the cortical sites which reflects the differences in anatomical site, surgical preparation, and biomechanical loading. Care should be taken when extrapolating osseointegration results for different clinical applications.

Radiographs and micro-computed tomography provided limited information with respect to the extent of osseointegration into the titanium alloy 3D-printed dowels interbody cage, while the radiographs demonstrated that the cages were well placed in the interbody space and subsidence was not an issue. Push-out testing of the dowels in the cortical bone clearly demonstrates the fixation achieved with bone ingrowth into porous materials and agrees with previous experience with this model with porous implants from traditional manufacturing techniques [9,12,16−18,48]. Spine stability based on ROM testing of the interbody fusions at 12 weeks at 7.5 Nm did not differ with autograft or supercritical fluid-treated allograft in the cage aperture.

Histology in the cortical sites demonstrated the open architecture of the 3D porous implants and osseointegration does progress with time. In contrast, the histology in cancellous sites like the interbody fusion sites had limited osseointegration. This cancellous site histology for porous devices agrees with our previous work [17] and may be due, in part, to anatomical loading and mechanical properties of the device. Interbody fusion histology revealed the importance of the aperture to support new bone formation from one level to the next for a fusion with autograft and supercritical fluid-treated allograft supporting new bone formation. The porous domains of the 3D-printed device in general were filled with fibrovascular tissue while some bone integration was found at 12 weeks when fusion within the aperture was present. This highlights the importance of the aperture with graft material and biomechanical stability which may play a role in driving further osseointegration.

The choice of hardware as well as graft material remains a complex issue for spinal fusion [14]. Sheep have been used for preclinical models to evaluate spinal fusion and provide insight for human use [25,37,38,41−45,59,60] but have their limitations. We used an endplate-sparing technique, which mimics the human interbody fusion technique, recently reported by Bae et al. [43], interbody cages with dimensions appropriate for the L4−L5 levels in sheep and posterior pedicle screw fixation. This is in contrast to other studies that either used a single lateral rod construct [43] or implants that were too large for the interbody space and a surgical technique that resulted in implants being placed in the vertebral body [38,41], which is not reflective of the technique used for human implantation. Differences in surgical preparation, implant dimensions, and the stability of the biomechanical environment will all influence the results. The short-term follow-up (bone dowels at 4 and 12 weeks and interbody fusions at 12 weeks) is limiting and may not reflect the long-term results with these types of implants where continued bone remodeling may reveal other results. We also did not examine any other porous implant designs or manufacturing methods. Care should be taken when extrapolating preclinical results and must consider surgical, implant, and biomechanical factors to fully appreciate the results.

References

[1] Albrektsson T, Albrektsson B. Osseointegration of bone implants: a review of an alternative mode of fixation. Acta Orthopaedica Scandinavica 1987;58:567–77.

[2] Albrektsson T, Brånemark P-I, Hansson H-A, Lindström J. Osseointegrated titanium implants: requirements for ensuring a long-lasting, direct bone-to-implant anchorage in man. Acta Orthopaedica Scandinavica 1981;52:155–70.

[3] Albrektsson T, Jansson T, Lekholm U. Osseointegrated dental implants. Dent Clin North Am 1986;30:151–74.

[4] Branemark P-I. Osseointegration and its experimental background. J Prosthet Dent 1983;50:399–410.

[5] Branemark R, Branemark P, Rydevik B, Myers RR. Osseointegration in skeletal reconstruction and rehabilitation: a review. J Rehabil Res Dev 2001;38:175–82.

[6] Goto T. Osseointegration and dental implants. Clin Calcium 2014;24:265–71.

[7] Pellegrini G, Francetti L, Barbaro B, del Fabbro M. Novel surfaces and osseointegration in implant dentistry. J Investig Clin Dent 2018;9:1–9.

[8] Bobyn J, Pilliar R, Cameron H, Weatherly G. The optimum pore size for the fixation of porous-surfaced metal implants by the ingrowth of bone. Clin Orthop Relat Res 1980(150):263–70.

[9] Bobyn J, Stackpool G, Hacking S, Tanzer M, Krygier J. Characteristics of bone ingrowth and interface mechanics of a new porous tantalum biomaterial. J Bone Joint Surg Br Vol 1999;81:907–14.

[10] Camron H, Pilliar R, Macnab I. The rate of bone ingrowth into porous metal. J Biomed Mater Res 1976;10:295–302.

[11] Kienapfel H, Sprey C, Wilke A, Griss P. Implant fixation by bone ingrowth. J Arthroplast 1999;14:355–68.

[12] Svehla M, Morberg P, Zicat B, Bruce W, Sonnabend D, Walsh WR. Morphometric and mechanical evaluation of titanium implant integration: comparison of five surface structures. J Biomed Mater Res 2000;51:15–22.

[13] Jain S, Eltorai AE, Ruttiman R, Daniels AH. Advances in spinal interbody cages. Orthop Surg 2016;8:278–84.

[14] Rao PJ, Pelletier MH, Walsh WR, Mobbs RJ. Spine interbody implants: material selection and modification, functionalization and bioactivation of surfaces to improve osseointegration. Orthop Surg 2014;6:81–9.

[15] Branemark P-I. Osseointegrated implants in the treatment of the edentulous jaw. Experience from a 10-year period. Scand J Plast Reconstr Surg Suppl 1977;16:1–132.

[16] Bertollo N, Da Assuncao R, Hancock NJ, Lau A, Walsh WR. Influence of electron beam melting manufactured implants on ingrowth and shear strength in an ovine model [epub ahead of print] [Record Supplied by Publisher]. J Arthroplasty 2012;27:1429–36.

[17] Bertollo N, Matsubara M, Shinoda T, Chen D, Kumar M, Walsh WR. Effect of surgical fit on integration of cancellous bone and implant cortical bone shear strength for a porous titanium. J Arthroplast 2011;26:1000–7.

[18] Bertollo N, Sandrini E, Pria PD, Walsh WR. Osseointegration of multiphase anodic spark deposition treated porous titanium implants in an ovine model. J Arthroplast 2015;30:484–8.

[19] Chen D, Bertollo N, Lau A, Taki N, Nishino T, Mishima H, et al. Osseointegration of porous titanium implants with and without electrochemically deposited DCPD coating in an ovine model. J Orthop Surg Res 2011;6:56.

[20] Le Guéhennec L, Soueidan A, Layrolle P, Amouriq Y. Surface treatments of titanium dental implants for rapid osseointegration. Dent Mater 2007;23:844–54.

[21] Mavrogenis A, Dimitriou R, Parvizi J, Babis G. Biology of implant osseointegration. J Musculoskelet Neuronal Interact 2009;9:61–71.

[22] Svehla M, Morberg P, Bruce W, Zicat B, Walsh WR. The effect of substrate roughness and hydroxyapatite coating thickness on implant shear strength. J Arthroplast 2002;17:304–11.

[23] Sykaras N, Iacopino AM, Marker VA, Triplett RG, Woody RD. Implant materials, designs, and surface topographies: their effect on osseointegration. A literature review. Int J Oral Maxillofac Implant 2000;15:675–90.

[24] Walsh WR, Bertollo N, Christou C, Schaffner D, Mobbs RJ. Plasma-sprayed titanium coating to polyetheretherketone improves the bone-implant interface. Spine J 2015;15:1041–9.

[25] Walsh WR, Pelletier MH, Bertollo N, Christou C, Tan C. Does PEEK/HA enhance bone formation compared with PEEK in a sheep cervical fusion model? Clin Orthop Relat Res 2016;474:2364–72.
[26] Walsh WR, Pelletier MH, Christou C, He J, Vizesi F, Boden SD. The in vivo response to a novel Ti coating compared with polyether ether ketone: evaluation of the periphery and inner surfaces of an implant. Spine J 2018;18:1231–40.
[27] Schmalzried TP, Harris W. The Harris-Galante porous-coated acetabular component with screw fixation. Radiographic analysis of eighty-three primary hip replacements at a minimum of five years. J Bone Joint Surg Am Vol 1992;74:1130–9.
[28] Guedes e Silva CC, Konig Jr. B, Carbonari MJ, Yoshimoto M, Allegrini Jr. S, Bressiani JC. Tissue response around silicon nitride implants in rabbits. J Biomed Mater Res A 2008;84:337–43.
[29] Mobbs RJ, Rao PJ, Phan K, Hardcastle P, Choy WJ, McCartney ER, et al. Anterior lumbar interbody fusion using reaction bonded silicon nitride implants: long term case series of the first synthetic ALIF spacer implanted in humans. World Neurosurg 2018;120:256–64.
[30] Ducheyne P, Aernoudt E, De Meester P, Martens M, Mulier JC, Van Leeuwen D. Factors governing the mechanical behavior of the implant-porous coating-trabecular bone interface. J Biomech 1978;11:297–307.
[31] Ducheyne P, De Meester P, Aernoudt E, Martens M, Mulier J. Influence of a functional dynamic loading on bone ingrowth into surface pores of orthopedic implants. J Biomed Mater Res 1977;11:811–38.
[32] Kasliwal MK, Baskin DS, Traynelis VC. Failure of porous tantalum cervical interbody fusion devices: two-year results from a prospective, randomized, multicenter clinical study. Clin Spine Surg 2013;26:239–45.
[33] Zou X, Li H, Bünger M, Egund N, Lind M, Bünger C. Bone ingrowth characteristics of porous tantalum and carbon fiber interbody devices: an experimental study in pigs. Spine J 2004;4:99–105.
[34] Han C-M, Lee E-J, Kim H-E, Koh Y-H, Kim KN, Ha Y, et al. The electron beam deposition of titanium on polyetheretherketone (PEEK) and the resulting enhanced biological properties. Biomaterials 2010;31:3465–70.
[35] Walsh WR, Bertollo N, Christou C, Schaffner D, Mobbs R. Plasma sprayed titanium coating to PEEK improves the bone-implant interface. Spine J 2014 S1529-9430(14)01874-9. https://doi.org/10.1016/j.spinee.2014.12.018.
[36] Guyer RD, Abitbol J-J, Ohnmeiss DD, Yao C. Evaluating osseointegration into a deeply porous titanium scaffold: a biomechanical comparison with PEEK and allograft. Spine 2016;41:E1146–50.
[37] Pelletier MH, Cordaro N, Punjabi VM, Waites M, Lau A, Walsh WR. PEEK versus Ti interbody fusion devices: resultant fusion, bone apposition, initial and 26-week biomechanics. Clin Spine Surg 2016;29:E208–14.
[38] McGilvray KC, Waldorff EI, Easley J, Seim HB, Zhang N, Linovitz RJ, et al. Evaluation of a polyetheretherketone (PEEK) titanium composite interbody spacer in an ovine lumbar interbody fusion model: biomechanical, microcomputed tomographic, and histologic analyses. Spine J 2017;17(12):1907–16.
[39] Tsou H-K, Chi M-H, Hung Y-W, Chung C-J, He J-L. In vivo osseointegration performance of titanium dioxide coating modified polyetheretherketone using arc ion plating for spinal implant application. Biomed Res Int 2015;2015:1–9.
[40] Wang X, Xu S, Zhou S, Xu W, Leary M, Choong P, et al. Topological design and additive manufacturing of porous metals for bone scaffolds and orthopaedic implants: a review. Biomaterials 2016;83:127–41.
[41] McGilvray KC, Easley J, Seim HB, Regan D, Berven SH, Hsu WK, et al. Bony ingrowth potential of 3D-printed porous titanium alloy: a direct comparison of interbody cage materials in an in vivo ovine lumbar fusion model. Spine J 2018;18:1250–60.
[42] Lindley EM, Barton C, Blount T, Burger EL, Cain CM, Seim HB, et al. An analysis of spine fusion outcomes in sheep pre-clinical models. Eur Spine J 2017;26:228–39.
[43] Bae HW, Patel VV, Sardar ZM, Badura JM, Pradhan BB, Seim III HB, et al. Transient local bone remodeling effects of rhBMP-2 in an ovine interbody spine fusion model. JBJS 2016;98:2061–70.
[44] Wu SH, Li Y, Zhang YQ, Li XK, Yuan CF, Hao YL, et al. Porous titanium−6 aluminum−4 vanadium cage has better osseointegration and less micromotion than a poly−ether−ether−ketone cage in sheep vertebral fusion. Artif Org 2013;37:E191–201.
[45] Siu RK, Lu SS, Li W, Whang J, McNeill G, Zhang X, et al. Nell-1 protein promotes bone formation in a sheep spinal fusion model. Tissue Eng Part A 2011;17:1123–35.
[46] Toth JM, Wang M, Scifert JL, Cornwall GB, Estes BT, Seim HB, et al. Evaluation of 70/30 D, L-PLa for use as a resorbable interbody fusion cage. Orthopedics 2002;25:S1131–S40.
[47] Sandhu HS, Toth JM, Diwan AD, Seim III H, Kanim LE, Kabo JM, et al. Histologic evaluation of the efficacy of rhBMP-2 compared with autograft bone in sheep spinal anterior interbody fusion. Spine 2002;27:567–75.
[48] Svehla M, Morberg P, Bruce W, Walsh WR. No effect of a type I collagen gel coating in uncemented implant fixation. J Biomed Mater Res Part B Appl Biomater 2005;74:423–8.
[49] Walsh WR, Loefler A, Nicklin S, Arm D, Stanford RE, Yu Y, et al. Spinal fusion using an autologous growth factor gel and a porous resorbable ceramic. Eur Spine J 2004;18:18.
[50] Walsh WR, Harrison J, Loefler A, Martin T, Van Sickle D, Brown MK, et al. Mechanical and histologic evaluation of collagraft in an ovine lumbar fusion model. Clin Orthop 2000(375):258–66.
[51] van Dijk LA, Duan R, Luo X, Barbieri D, Pelletier M, Christou C, et al. Biphasic calcium phosphate with submicron surface topography in an ovine model of instrumented posterolateral spinal fusion. JOR Spine 2018:e1039.
[52] Christou C, Oliver RA, Rawlinson J, Walsh WR. Transdermal fentanyl and its use in ovine surgery. Res Vet Sci 2015;100:252–6.
[53] Yuan H, Fernandes H, Habibovic P, de Boer J, Barradas AM, de Ruiter A, et al. Osteoinductive ceramics as a synthetic alternative to autologous bone grafting. Proc Natl Acad Sci 2010;107:13614–9.
[54] Mobbs RJ, Phan K, Assem Y, Pelletier M, Walsh WR. Combination Ti/PEEK ALIF cage for anterior lumbar interbody fusion: early clinical and radiological results. J Clin Neurosci 2016;34:94–9.
[55] Mobbs RJ, Parr WC, Choy WJ, McEvoy A, Walsh WR, Phan K. Anterior lumbar interbody fusion using a personalized approach: is custom the future of implants for anterior lumbar interbody fusion surgery? World Neurosurg 2019;124:452–8.
[56] Choy WJ, Parr WC, Phan K, Walsh WR, Mobbs RJ. 3-dimensional printing for anterior cervical surgery: a review. J Spine Surg 2018;4:757.
[57] Chong E, Mobbs RJ, Pelletier MH, Walsh WR. Titanium/polyetheretherketone cages for cervical arthrodesis with degenerative and traumatic pathologies: early clinical outcomes and fusion rates. Orthop Surg 2016;8:19–26.
[58] Phan K, Pelletier MH, Rao PJ, Choy WJ, Walsh WR, Mobbs RJ. Integral fixation titanium/polyetheretherketone cages for cervical arthrodesis: evolution of cage design and early radiological outcomes and fusion rates. Orthop Surg 2019;11:52–9.
[59] Gadomski BC, McGilvray KC, Easley JT, Palmer RH, Ehrhart E, Haussler KK, et al. An in vivo ovine model of bone tissue alterations in simulated microgravity conditions. J Biomech Eng 2014;136:021020.
[60] Gadomski BC, McGilvray KC, Easley JT, Palmer RH, Santoni BG, Puttlitz CM. Partial gravity unloading inhibits bone healing responses in a large animal model. J Biomech 2014;47:2836–42.